# COMBINED RIDGE-STEIN ESTIMATOR IN EXTERIOR ORIENTATION FOR LINEAR PUSHBROOM IMAGERY

Wang Tao, Zhang Yong-sheng, Zhang Yan

Department of Remote Sensing Information Engineering, Zhengzhou Institute of Surveying and Mapping, No. 66 Longhai Middle Road, Zhengzhou City 450052, Henan Province,China - wt4289@sina.com; zy4289@sina.com

**Commission IV, WG IV/7**

**KEY WORDS:** exterior, orientation, pushbroom, estimation, algorithm, accuracy

**ABSTRACT:**

The paper presents the combined ridge-stein estimator (CRS) for linear pushbroom imagery exterior orientation, which is severely ill-conditioned for the strong correlation among exterior orientation elements of linear pushbroom imagery. The estimator is a new biased method combining the ridge estimator and the stein estimator. It can effectively change the ill-conditioned state of linear pushbroom imagery exterior orientation process and achieve optimum estimation values through applying different scale compression to each least squares estimation component. Its performance is evaluated using one 10-meter SPOT 1 panchromatic image and one 2.5-meter SPOT 5 panchromatic image. Experimental results show that the combined ridge-stein estimator can effectively overcome the strong correlation among exterior orientation elements and reach high reliability, stability and accuracy. It is within one pixel accurate for ground directional points and within one and a half pixels accurate for ground check points.

## 1. INTRODUCTION

The linear pushbroom imagery is widely used in remote sensing mapping for its stable geometry and good image quality, such as SPOT, MOMS-02, IRS-1C/D and IKONOS images. However, the strong correlation among exterior orientation elements of this kind image induces normal equation heavily ill-conditioned (Gupta, 1997) and severely affects the reliability, stability and precision properties of exterior orientation.

Aiming at solving this problem many researchers have put forward different methods, including the incorporation of high-correlated elements, the separate and iterative solution of line elements and angle elements, the fictitious error equation, the ridge estimator (Huang, 1992; Zhang, 1989), the stein estimator (Zhang, 1989) and so. But there lie various shortcomings among these methods. The incorporation of high-correlated elements method only works well when the photography state is near to vertical photography. The separate and iterative solution of line elements and angle elements method isn't rigorous in theory and the orientation precision and iterative times depend on the accuracy of initial exterior orientation elements. The fictitious error equation method adds great workload and demands much ancillary data, such as orbit parameters, satellite photo data, and etc. The ridge estimator (Guo, 2002) and the stein estimator are both biased methods and can achieve better results than those unbiased estimation methods listed before. However, the two methods still need improvements. The ridge estimator has not a unique solution for it is non-linear to its estimation parameter. The stein estimator applies the same scale compression to each least squares estimation element without considering the fact that each element has different sized error. Therefore, in this paper the combined ridge-stein estimator (CRS) (Gui, 2002) is proposed up for linear pushbroom imagery exterior orientation. The CRS estimator is new biased estimator and has never been applied to photography before.

In the following, after a brief introduction of the CRS estimator, focus is put on its application in the linear pushbroom imagery exterior orientation, and then experiments are performed using one 10-meter SPOT 1 panchromatic image and one 2.5-meter SPOT 5 panchromatic image, and finally conclusion is drawn.

## 2. DEFINITION OF THE COMBINED RIDGE-STEIN ESTIMATOR AND ITS PROPERTIES

In the adjustment for the unknown $X$ the following observation equation can be established, and mean square error (MSE) is adopted to assess the accuracy of the estimation value $\hat{X}$. The smaller the MSE is, the more accurate the estimation value is.

$$V = AX - L \quad E(V) = 0, Cov(V) = \sigma_0^2 P^{-1} \tag{1}$$

$$MSE(\hat{X}) = \sigma_0^2 \sum_{i=2}^{t} 1/\lambda_i + \sum_{i=1}^{t} \left(E(\hat{X}_i) - X_i\right)^2 \tag{2}$$

where $A$ = coefficient matrix (n row × t column)
$L$ = constant matrix (n row × 1 column)
$V$ = residual matrix (n row × 1 column)
n = the number of observed values
t = the number of unknowns
$\sigma_0^2$ = variance of unit weight
$\lambda_i$ = the ith eigenvalue in the eigenvalue matrix

The least squares estimation, the ridge estimation and the stein estimation for the parameter $X$ are respectively:

$$\hat{X}_{LS} = (A^T PA)^{-1} A^T PL \quad (3)$$

$$\hat{X}_R(k) = (A^T PA + KI)^{-1} A^T PL \quad (4)$$

$$\hat{X}_{Stein}(c) = c(A^T PA)^{-1} A^T PL \quad (5)$$

where $\hat{X}_{LS}$ = least squares (LS) estimation value

$\hat{X}_R(K)$ = ridge estimation value

$\hat{X}_{Stein}(c)$ = stein estimation value

$I$ = unit matrix

$K$ = the ridge parameter vector $(K_i > 0)$

$c$ = the stein parameter( $c > 0$ )

If each element in vector $K$ is equal, the ridge estimator is regarded as the ordinary ridge estimator; else the ridge estimator is deemed as the generalized ridge estimator. The second item in equation (2) is constantly zero for the least square estimator since it is an unbiased estimator. But for the ridge estimator and the stein estimator the second item is no longer zero since they are biased estimators.

The combined ridge-stein estimator can be represented below:

$$\begin{aligned}\hat{X}_{CRS}(d) &= (A^T PA + I)^{-1}(A^T PL + dI)\hat{X}_{LS} \\ &= Q(\Lambda + I)^{-1}(\Lambda + dI)Q^T \hat{X}_{LS}\end{aligned} \quad (6)$$

where $Q$ = eigenvector matrix

$\Lambda$ = eigenvalue matrix

$d$ = the CRS parameter , $0 < d < 1$

The CRS estimator possesses three favorable characteristics in comparison with the ridge estimator and the stein estimator.

(1) The CRS estimator is more accurate than the ridge estimator and the stein estimator.

From the viewpoint of statistics a good estimation value should have a minor MSE. The MSE value of the CRS estimator is smaller than the ridge estimator and the stein estimator when $d$ is optimum, therefore, the CRS estimator is more accurate.

(2) The CRS estimator is superior to the ridge estimator and the stein estimator in reliability and stability.

To get correct and accurate estimation results, the ill-conditioned state of the normal equation must be changed. The CRS estimator alters the ill-conditioned state much more significantly than the ridge estimator and the stein estimator, therefore, its reliability and stability are more excellent.

(3) The solution for the CRS estimator is unique and simple.

Since the CRS estimator is a linear function to its estimation parameter, the optimal value for $d$ is ascertained when $MSE\left(\hat{X}_{CRS}\right)' = 0$.

$$d = \sum_{i=1}^{n} \frac{\hat{Y}^2_{CRS(i)}(d) - \hat{\sigma}_0^2}{(\lambda_i + 1)^2} \Bigg/ \sum_{i=1}^{n} \frac{\hat{\sigma}_0^2 + \lambda_i \hat{Y}^2_{CRS(i)}(d)}{\lambda_i (\lambda_i + 1)^2} \quad (7)$$

where $\hat{Y}_{CRS(i)}(d)$ is the canonical value for $\hat{X}_{CRS(i)}(d)$ ,which is imported to facilitate and simplify computation.

$$\hat{Y} = Q^T \hat{X} \quad (8)$$

$$\hat{Y}_{CRS}(d) = Q^T \hat{X}_{CRS}(d) = (\Lambda + I)^{-1}(\Lambda + dI)\Lambda^{-1}(AQ)^T L \quad (9)$$

## 3. THE CRS ESTIMATOR'S APPLICATION IN LINEAR PUSHBROOM IMAGERY EXTERIOR ORIENTATION

### 3.1 Theoretical Basis

This paragraph is mainly concerned with how to apply the CRS estimator in linear pushbroom imagery exterior orientation. The linear pushbroom imagery has multiple perspective centers and each scan line has an unique set of perspective center and rotation angles. The collinearity equation between a image pixel on the ith scan line ($x_i$, 0) and its corresponding object point in the object spcae ($X$, $Y$, $Z$) is as follows:

$$\left.\begin{aligned} x_i &= -f\frac{a_1(X-X_{si})+b_1(Y-Y_{si})+c_1(Z-Z_{si})}{a_3(X-X_{si})+b_3(Y-Y_{si})+c_3(Z-Z_{si})} \\ 0 &= -f\frac{a_2(X-X_{si})+b_2(Y-Y_{si})+c_2(Z-Z_{si})}{a_3(X-X_{si})+b_3(Y-Y_{si})+c_3(Z-Z_{si})} \end{aligned}\right\} \quad (10)$$

The $y$ coordinate along the flight direction is implied in the position and attitude of the satellite at a given time, which can be linearly related to the location and attitude of the central linear array as follows:

$$\left.\begin{aligned} \varphi_i &= \varphi_0 + \dot{\varphi}\cdot y \\ \omega_i &= \omega_0 + \dot{\omega}\cdot y \\ \kappa_i &= \kappa_0 + \dot{\kappa}\cdot y \\ X_{si} &= X_{S0} + \dot{X}_s \cdot y \\ Y_{si} &= Y_{S0} + \dot{Y}\cdot y \\ Z_{si} &= Z_{S0} + \dot{Z}_s \cdot y \end{aligned}\right\} \quad (11)$$

where $f$ = focal length

$\varphi_0, \omega_0, \kappa_0, X_{s0}, Y_{s0}, Z_{s0}$ = exterior orientation elements of the central scan line

$\varphi_i, \omega_i, \kappa_i, X_{si}, Y_{si}, Z_{si}$ = exterior orientation elements of the ith scan line

$a_i$, $b_i$, $c_i$ = elements of rotation matrix

$\dot{\varphi}, \dot{\omega}, \dot{\kappa}, \dot{X}_s, \dot{Y}_s, \dot{Z}_s$ = variation rates of exterior orientation elements.

Each scene has 12 exterior elemets ( $\varphi_0, \omega_0, \kappa_0, X_{s0}, Y_{s0}, Z_{s0}$ , $\dot{\varphi}, \dot{\omega}, \dot{\kappa}, \dot{X}_s, \dot{Y}_s, \dot{Z}_s$ ). Among them $X_{si}$ and $\varphi_i$ , $Y_{si}$ and $\omega_i$ are highly correlated. A small change in $\varphi_i$ is indistinguishable from a small change in $X_{si}$ . Similarly, small changes in $Y_{si}$ and $\omega_i$ can't be differentiated either. The strong correlation induces the coefficient matrix of the normal equation $A^T PA$ singular, the normal equation ill-conditioned and some eigenvalues $\lambda_i$ in the eigenvalue matrix $\Lambda$ close to zero as well. Accordingly, the

MSE value of least square estimation value $\hat{X}_{LS}$ become very large and least square estimator is no more an optimum estimator.

The ridge estimator and the stein estimator succeed in reducing the first item $\sigma_0^2 \sum_{i=2}^{t} 1/\lambda_i$ together with the total MSE value In equation (2) at the expense of increasing the second item $\sum_{i=1}^{t} \left(E\left(\hat{X}_i\right) - X_i\right)^2$. In equation (4) the ridge estimator alters the ill-conditioned state of the normal equation by using $A^T PA + KI$ to take place $A^T PA$. By adding a small positive value $K_i$, the eigenvalue $\lambda_i$ which is near to zero goes up to $\lambda_i + K_i$ and the least square estimation component $\hat{X}_{LS(i)}$ is compressed toward the origin point on the scale of $\lambda_i / (\lambda_i + K_i)$. Consequenly, the first item in MSE together with the total MSE drop greatly and the accuracy of estimation value is enhanced. The stein estimator reduces the MSE value and improves the estimation accuracy through compressing $\hat{X}_{LS(i)}$ value on the fixed scale $c$. However, because the ridge estimator is not a linear function to its estimation parameter $K$, it hasn't a unique and optimum solution approach, which results in its unreliability and instability. The common approaches for speculating the ridge estimator include Horel-Kennad method, Horel-Baldwin method, Lawless-Wang method and Mcdonald-Galarneau method. The stein estimator compresses each component of the least square estimation value on the same scale $c$ without considering the fact that each component has different sized error. Therefore, the components with big errors, i.e. the components corresponding to infinitesimal eigenvalues, don't get adequate compression and the precision of the stein estimator is limited.

In the CRS estimator $(A^T PA + I)(A^T PL + dI)^{-1}$ is substituted for $A^T PA$. The eigenvalue $\lambda_i$ rises to $\lambda_i (\lambda_i + 1)/(\lambda_i + d)$ and the least square estimation component $\hat{X}_{LS(i)}$ is compressed toward the origin point on the scale of $(\lambda_i + d)/(\lambda_i + 1)$. For the infinitesimal eigenvalue, the new eigenvalue is near to $\lambda_i / d$, augmented tens, hundreds, or maybe thousands of times. At the same time the component corresponding to the infinitesimal eigenvalue, i.e. the component with large error, is compressed on the scale of near to $d$, while the component corresponding to the large eigenvalue, i.e. the component with minor error, remains nearly unchanged. Hence, it can be concluded that the CRS estimator changes the ill-conditioned state of the normal equation more significantly and more rationally. Moreover, it can be also testified that the CRS estimator is the most accurate in MSE meaning by comparing MSE values of the CRS estimator, the ridge estimator and the stein estimator.

### 3.2 Calculation Process

The exterior orientation process for linear pushbroom imagery by the CRS estimator can be divided into several steps:
Step 1: Computation of the initial values of exterior orientation elements $\hat{X}_0$.

Step 2: Computation of the least square estimation value $\hat{X}_{LS}$ and its corresponding canonical value $\hat{Y}_{LS}$.

First, coefficient matrix $A$, residual matrix $V$ should be constructed, and then normal equation is established, and finally $\hat{X}_{LS}$ is computed according to equation (1).

Step 3: Computation of the CRS parameter $d$.

The parameter $d$ should be computed by equation (7). Because the parameter $d$ and the value $\hat{Y}_{CRS}(d)$ are inter-determined, the solution for parameter $d$ is an iterative process. For the first time, $\hat{Y}_{LS}$ is used to replace $\hat{Y}_{CRS}(d)$ in equation (7) to calculate the first iterative value $d_0$, and then $d_0$ is used to calculate $\hat{Y}_{CRS}(d_0)$ inversely; for the next time $\hat{Y}_{CRS}(d_0)$ is used to calculate $d_1$ and $d_1$ is used to calculate $\hat{Y}_{CRS}(d_1)$; the process will continue on until $\left|d_j - d_{j+1}\right| < \varepsilon$ ($\varepsilon$ is the tolerance).

Step 4: Computation of the CRS estimation value $\hat{X}_{CRS}{}^{i}(d)$ according to equation (6). The superscript $i$ denotes the ith circulation time in the whole process.

Step 5: Updating the exterior orientation elements $\hat{X}_i = \hat{X}_{i-1} + \hat{X}_{CRS}{}^{i}(d)$.

Step 6: Judgement is put on $\hat{X}_{CRS}{}^{i}(d)$ to see if it is smaller than the threshold value. If $\hat{X}_{CRS}{}^{i}(d)$ is smaller than the threshold value, $\hat{X}_i$ is the ultimate exterior elements. If $\hat{X}_{CRS}{}^{i}(d)$ is bigger than threshold value, the next circulation process will repeat from step 2. Iterative circulation won't end unless $\hat{X}_{CRS}{}^{i}(d)$ is smaller than the threshold value.

## 4. EXPERIMENTAL RESULTS AND EVALUATION

### 4.1 Test Data Sets

The test fields comprise two data sets. The first data set is a panchromatic SPOT 1 1A image taken in northern China in 1986, named as Image 01. The image contains 6000□6000 pixels and covers 60□60 ground square kilometers, the northern and northern-eastern parts of the image are mountains, the central part is urban city and the other parts are predominantly rural with land use. The ground elevation range varies from about -50 to about 550 meters. The sun angle azimuth is 140.6°, the sun angle elevation is 64.60°, the principal distance of the sensor is 1082 millimeters, the film pixel size is 13 microns, and the ground resolution is 10 meters. 57 well-defined control points were measured from 1:50,000-scale maps, among them 18 control points are used as directional points and the left points are used as check points. Figure 1 illustrates the coverage area of the image with the ground points distribution. Triangles represent directional points and circles represent check points.

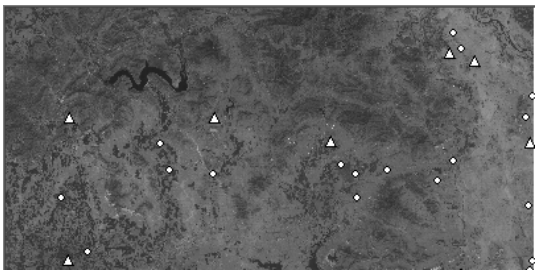

The second test field is a panchromatic SPOT 5 image taken in another place in northern China in 2002, named as Image 02. The image contains 24000□24000 pixels and covers 6000□6000 ground square kilometers. The northwest and southeast parts of image are urban areas and the other parts are mainly mountains. The ground height varies between about 10 to about 1550 meters. The sun angle azimuth is 166.7070°, the sun angle elevation is 28.2098°, the principal distance of the sensor is 1082 millimeters, the film pixel size is 3.25 microns, and the ground resolution is 2.5 meters. 33 well-defined control points were measured from 1:25,000-scale maps, 13 as directional points and 20 as check points. Figure 2 illustrates the coverage area of the image with the ground points distribution. Triangles represent directional points and circles represent check points.

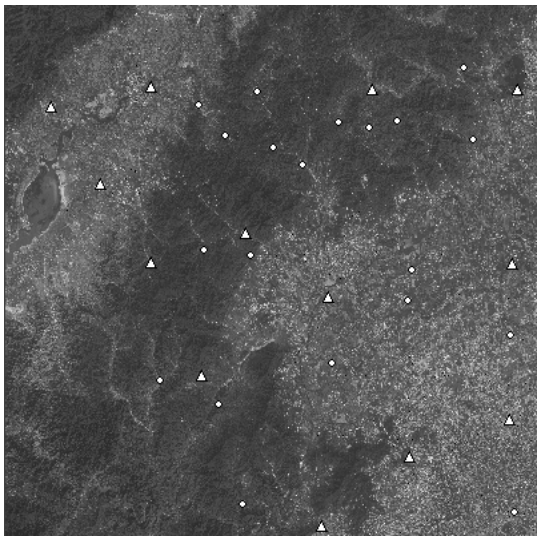

Figure 2. SPOT Image 02

### 4.2 Results and Evaluation

The least square estimator, the stein estimator, the ordinary ridge estimator with Horel-Kennad and Lawless-Wang approaches, the generalized ridge estimate and the combined ridge-stein estimator are used to compute exterior elements for these two SPOT scenes. LS refers to the least square estimator, Stein refers to the stein estimator, HK refers to the ordinary ridge estimator with Horel-Kennad approach, LW refers to the ordinary ridge estimator with Lawless-Wang approach, GR refers to the generalized ridge estimator and CRS refers to the combined ridge-stein estimator.

Root mean square errors (RMSE) in the image photo coordinates and the ground space coordinates are taken to evaluate precision of different orientation methods. *vox*, *voy*, *Vox*, *Voy* and *Voz* represent directional points' RMSE in the image photo coordinates *x*□*y* and object space coordinates *X*, *Y* and Z respectively. And *vcx*, *vcy*, *Vcx*, *Vcy* and *Vcz* have the same meaning for check points.

For test data Image 01 Table 1 and Table 2 show RMSE at directional points and check points respectively.

Unit: pixel(p) and meter(m)

| Method | *vox/p* | *voy/p* | *Vox/m* | *Voy/m* | *Voz/m* |
|---|---|---|---|---|---|
| LS | 61.80 | 20.10 | 715.67 | 217.82 | 30.16 |
| Stein | 1.07 | 1.20 | 8.27 | 10.88 | 7.35 |
| HK | 1.05 | 1.21 | 8.18 | 10.82 | 7.34 |
| LW | 51.88 | 10.92 | 660.22 | 112.73 | 25.53 |
| GR | 0.98 | 1.01 | 7.66 | 10.07 | 7.33 |
| CRS | 0.82 | 0.91 | 5.67 | 8.51 | 7.32 |

Table 1. Test results at directional points for Image 01

Unit: pixel(p) and meter(m)

| Method | *vcx/p* | *vcy/p* | *Vcx/m* | *Vcy/m* | *Vcz/m* |
|---|---|---|---|---|---|
| LS | 72.37 | 26.68 | 722.34 | 125.62 | 22.30 |
| Stein | 1.54 | 1.67 | 13.92 | 15.14 | 7.85 |
| HK | 1.49 | 1.66 | 13.70 | 14.89 | 7.85 |
| LW | 61.75 | 12.13 | 675.49 | 111.88 | 20.71 |
| GR | 1.30 | 1.41 | 13.48 | 14.43 | 7.84 |
| CRS | 1.23 | 1.38 | 13.16 | 13.73 | 7.58 |

Table 2. Test results at check points for Image 01

For test data Image 02 Table 3 and Table 4 show RMSE at directional points and check points respectively.

Unit: pixel(p) and meter(m)

| Method | *vox/p* | *voy/p* | *Vox/m* | *Voy/m* | *Voz/m* |
|---|---|---|---|---|---|
| LS | 1.23 | 1.26 | 4.11 | 4.66 | 5.40 |
| Stein | 0.46 | 0.27 | 2.90 | 2.26 | 1.99 |
| HK | 0.44 | 0.26 | 2.78 | 2.25 | 1.99 |
| LW | 105.81 | 134.40 | 770.7 | 745.3 | 123.32 |
| GR | 0.41 | 0.23 | 2.69 | 2.22 | 1.98 |
| CRS | 0.22 | 0.20 | 2.02 | 1.80 | 1.54 |

Table 3. Test result at directional points for Image 02

Unit: pixel(p) and meter(m)

| Method | *vcx/p* | *vcy/p* | *Vcx/m* | *Vcy/m* | *Vcz/m* |
|---|---|---|---|---|---|
| LS | 2.24 | 2.23 | 7.38 | 7.29 | 10.13 |
| Stein | 1.65 | 1.52 | 5.48 | 5.07 | 4.57 |
| HK | 1.62 | 1.49 | 5.49 | 4.97 | 4.52 |
| LW | 921.67 | 140.75 | 2432.58 | 837.9 | 50.45 |
| GR | 1.61 | 1.43 | 5.39 | 4.88 | 4.50 |
| CRS | 1.41 | 1.33 | 4.47 | 4.34 | 4.39 |

Table 4. Test results at check points for Image 02

Table 1,Table 2,Table 3 and Table 4 show that the CRS estimator is the most accurate, for both 10 meter resolution SPOT 1 image and 2.5 resolution SPOT 5 image the orientation precision at directional points is within one pixel and that at control points is with one and a half pixels. The next best estimators are the stein estimator, the ordinary ridge estimator with Horel-Kennad approach and the generalized ridge estimator, about one pixel accurate at directional points and two pixels accurate at check points. Among these three next best estimators the generalized ridge is slightly better than the ordinary ridge estimator with Horel-Kennad approach, and the latter is slightly better than the stein estimator. The least square estimator and the ordinary ridge estimator with Lawless-Wang approach are the worst, unstable and inaccurate.

Therefore, it can be concluded that the ridge-stein estimator is the most accurate, reliable and stable approach for linear pushbroom imagery orientation.

## 5. CONCLUSIONS

The strong correlation among exterior orientation elements of linear pushbroom imagery causes the normal equation ill-conditioned and least squares estimation values no longer optimal. The new biased estimator, the combined ridge-stein estimator can effectively overcome the ill-conditioned problem and improve orientation precision. Experimental results confirm that the CRS estimator is superior to the least square estimator, the ridge estimator and the stein estimator in accuracy, reliability and stability. The combined ridge-stein estimator is a perfect approach for linear pushbroom imagery orientation.

## REFERENCES


Gui, Q. M., Li, G. Z., 2002. Combined ridge with shrunken estimator and its application in geodetic adjustment. *Journal of Geodesy and Geodynamics*, 22(1), pp. 16-21.

Guo, H.T., Zhang, B. M., Gui Q.M., 2002. Application of generalized ridge estimation in computing the exterior orientation elements of satellitic linear array scanner imagery. In: *The International Archives of the Photogrammetry, Remote Sensing and Spatial Information Sciences*, Xi'an, China, Vol. XXXIV, Part 2, pp. 153-156.

Gupta, R., Hartley, R., 1997. Linear pushbroom cameras. *IEEE Trans. PAMI*, 19(9), pp.963-975.

Huang W. B., 1992. *Modern Adjustment Theory and Its Application*, Beijing Publishing House, Beijing, pp.120 -132.

Zhang, F. R., Wang X. Q., 1989. Ridge and stein estimation for adjustment parameters. *Journal of Wuhan Technical University of Surveying and Mapping*, 14(3), pp. 46-57.